Journal of Physiology (1992), **449**, *pp.* 759–783
With 12 *figures*
Printed in Great Britain

CATION INTERACTIONS WITHIN THE CYCLIC GMP-ACTIVATED CHANNEL OF RETINAL RODS FROM THE TIGER SALAMANDER

BY A. L. ZIMMERMAN* AND D. A. BAYLOR

*From the Department of Neurobiology, Sherman Fairchild Science Building, Stanford University School of Medicine, Stanford, CA 94305, USA and *the Section of Physiology, Brown University, Box G-B329, Providence, RI 02912, USA*

(*Received 18 June 1991*)

SUMMARY

1. The ionic dependence of current through the 3′,5′-cyclic guanosine monophosphate (cyclic GMP)-activated channels of salamander rods was studied in excised inside-out membrane patches from isolated outer segments. Voltage-clamp experiments on transducing rods were performed so that the channels in intact cells could be compared with those in excised patches.

2. The reversal potential of the cyclic GMP-induced patch current was close to the Na^+ equilibrium potential when the concentration of NaCl on the cytoplasmic surface of a patch was varied at constant external NaCl concentration. Fitting the Goldman–Hodgkin–Katz equation indicated that the apparent ratio of permeabilities for Na^+ and Cl^- was at least 50. This confirms a previous report that the channel's Na^+ permeability is much larger than its Cl^- permeability.

3. Na^+ currents through the channel did not obey the independence principle. The outward patch current at large positive potential began to saturate with increasing concentrations of internal Na^+, as if permeation required Na^+ to bind to a site with an apparent dissociation constant around 180 mM.

4. In symmetrical NaCl solutions containing very low concentrations of divalent cations the current–voltage relation measured from excised patches 50 μs after switching the voltage showed mild outward rectification. By 1 ms the rectification was more pronounced. The rectification at 50 μs is attributed to voltage dependence of Na^+ permeation. The additional rectification at later times is attributed to voltage dependence of the channel's probability of being open, depolarization favouring the open state.

5. In symmetrical Mg^{2+} solutions the cyclic GMP-induced patch currents were smaller and the outward rectification was more pronounced.

6. Addition of Mg^{2+} or Ca^{2+} to an internal Na^+ solution blocked the cyclic GMP-induced Na^+ current through the channels, as if by occupying a single binding site with an affinity in the 0·1–2 mM range. Block by Mg^{2+} was voltage dependent, suggesting that the binding site was within the channel's transmembrane electric field. Raising the Mg^{2+} concentration on the external surface of the patch increased

MS 9490

the apparent dissociation constant of block by internal Mg^{2+}, as expected if external and internal Mg^{2+} compete for the same binding site.

7. Block by internal Ca^{2+} had an opposite and weaker voltage dependence than block by internal Mg^{2+}.

8. In symmetrical solutions containing both Na^+ and Mg^{2+} the outward rectification was more pronounced than in solutions containing Na^+ alone. In solutions thought to be close to physiological the outward patch current increased e-fold for a depolarization of 24–30 mV. This voltage sensitivity approaches that of the light-sensitive current of intact rods.

9. As internal Na^+ was progressively replaced by Ca^{2+} the outward patch current at positive potential fell monotonically, with no sign of anomalous mole-fraction behaviour. There was thus no evidence that cationic conduction depended on repulsive electrostatic interactions between cations in the channel.

10. The results are in reasonable agreement with a simple model in which it is assumed that cations permeate and block the channel by combining with a single binding site located in the transmembrane electric field. While our results do not exclude other ion binding sites, they suggest that one site may dominate the permeation process.

INTRODUCTION

A cation-selective conductance controlled by 3′,5′-cyclic guanosine monophosphate (cyclic GMP) generates the electrical response to light in retinal rods (Fesenko, Kolesnikov & Lyubarsky, 1985; reviewed in Yau & Baylor, 1989). Physiological studies have shown that the molecular unit of the conductance is a water-filled pore rather than a carrier (Haynes, Kay & Yau, 1986; Zimmerman & Baylor, 1986) and that multiple cyclic GMP molecules bind to open the pore (Fesenko *et al.* 1985).

Although monovalent cations carry most of the light-regulated current in a transducing rod (Yau, McNaughton & Hodgkin, 1981), Ca^{2+} and Mg^{2+} ions permeate the open channel and block Na^+ fluxes through it. The block by divalent cations lowers the effective single-channel current by two to three orders of magnitude (Haynes *et al.* 1986; Zimmerman & Baylor, 1986), reducing channel noise in darkness and allowing single photon detection to occur. Ca^{2+} entry through open channels provides a measure of channel activation for the negative feedback loop that controls the internal concentration of cyclic GMP and mediates light adaptation (reviewed in Lamb & Pugh, 1990). Although the channel's molecular structure is not yet well understood, it has recently been cloned and expressed in frog oocytes (Kaupp, Niidome, Tanabe, Terada, Bonigk, Stuhmer, Cook, Kangawa, Matsuo, Hirose, Miyata & Numa, 1989).

We have approached the mechanisms of permeation and block in the channel by examining the ionic dependence of macroscopic currents through excised patches. The results suggest that ion permeation is controlled mainly by a single binding site in the channel at which cations pause during permeation, and that only one cation can occupy the site at a time. A simple model based on these assumptions gave a reasonable fit to results from several kinds of experiments. Analysing currents carried by monovalent cations, Menini (1990) also recently concluded that the channel

behaves primarily as a one-ion pore. Abstracts describing preliminary versions of this work have appeared (Zimmerman & Baylor, 1987, 1988).

METHODS

Experimental preparation

For experiments on excised patches, light-adapted larval tiger salamanders, *Ambystoma tigrinum*, were decapitated and pithed and the retinas isolated. Isolated rod outer segments were obtained by mechanically dissociating the retina under bright white light. While holding the outer segment with a suction electrode a patch electrode (borosilicate, Glass Company of America, Millville, NJ, USA) was sealed on the surface membrane. In some experiments, the suction electrode was omitted, and the bottom of the chamber was precoated with poly-L-lysine (1 mg ml^{-1} in water, then rinsed with Ringer solution) to immobilize outer segments during the approach of the patch electrode. Excision produced an 'inside-out' patch (Hamill, Marty, Neher, Sakmann & Sigworth, 1981; Fesenko *et al.* 1985). The patch electrodes had resistances of 3–5 MΩ when filled with isotonic NaCl solutions. Formation of a seal caused the pipette resistance to rise to 3–34 GΩ. A saturating concentration of cyclic GMP (typically 50–200 μM) was applied by perfusion of the chamber and the cyclic GMP-activated current obtained as the difference between currents recorded in the presence and absence of cyclic GMP. The leakage resistance was measured frequently during the experiment and usually changed little until the patch abruptly broke. Small cyclic GMP-induced currents were determined by subtracting the average of the leakage currents recorded just before and just after the current with cyclic GMP. About half of the freshly excised patches did not respond to cyclic GMP, apparently because excision produced a vesicle. Roughly half of these unresponsive patches responded to cyclic GMP after gently touching the tip of the pipette to a bead of Sylgard resin, which ruptured the vesicle. Experiments were performed at room temperature, 22–25 °C, under white light from the microscope illuminator and room lights.

A few experiments were performed on dark-adapted whole rods. For these experiments, the salamanders were dark-adapted for 2 h, and dissections and cell manipulations were performed under infra-red illumination. A suction electrode was used to hold the cell and collect the membrane current from the distal half of the outer segment, while the cell membrane potential was controlled using a patch electrode sealed onto the inner segment, with the patch ruptured. Current–voltage relations in the dark were compared with those in a steady, diffuse, saturating light at 530 nm.

Electrical recording

Currents from excised patches were measured with an Axopatch 1B patch-clamp amplifier (Axon Instruments, Burlingame, CA, USA). A PDP 11/73 computer and laboratory interface (Indec Systems, Sunnyvale, CA, USA) with software written in BASIC 23 were used to deliver voltage commands to the patch amplifier and to acquire and analyse the currents. Prior to acquisition the currents were processed with an 8-pole Bessel low-pass filter with selectable cut-off frequency (Frequency Devices, Haverhill, MA, USA). Aliasing was avoided by sampling at a rate 2–5 times the −3 dB frequency of the low-pass filter. Patch voltages were not corrected for the voltage drop in the series resistance of the pipette. For patches with the largest currents the true voltages would have been about 10% less than nominal. The analysis program was used to calculate the average currents in the presence and absence of cyclic GMP (typically ten to twenty trials each) and to subtract the averages.

For experiments on whole rods, the suction electrode current was recorded using a second patch-clamp amplifier. The output of this amplifier was stored on an FM tape-recorder (Hewlett Packard, Sunnyvale, CA, USA) and subsequently digitized. Series resistance was compensated electronically or calculated from the capacity currents and the membrane voltages subsequently corrected. All other electrical recording procedures were as for the excised-patch experiments.

Solutions

Light-adapted retinas were isolated and stored in modified amphibian Ringer solution consisting of (mM): NaCl, 111; KCl, 2·5; $CaCl_2$, 1·5; $MgCl_2$, 6; EDTA, 0·02; D-glucose, 10; HEPES buffer, 3 (pH 7·6). For experiments on whole rods, the patch pipette was filled with a pseudo-intracellular solution consisting of (mM): potassium aspartate, 76; KCl, 14; NaCl, 6; $MgCl_2$, 3; EDTA, 0·02; D-glucose, 10; sucrose, 27·5; K_2HPO_4, 2 (pH 7·6); ATP, 2; GTP, 1. For correlation with whole-cell

experiments, this same solution (without the ATP and GTP) was used in a few excised-patch experiments. All other excised-patch experiments were performed using a variety of solutions derived from a low-divalent solution consisting of: 130 mM-NaCl, 20 μM-EDTA and 1–10 mM-HEPES or Tris buffer (pH 7·6). Free Mg^{2+} was calculated to be $< 10^{-7}$ M and free $Ca^{2+} < 10^{-8}$ M. This solution was manipulated in various ways, such as by Na^+ substitution or addition of divalents, as indicated in the figure legends. For experiments on reduction of the Na^+ conductance by Mg^{2+} and Ca^{2+} (Figs 7 and 8), the divalents were buffered according to the methods described by Bartfai (1979). The solutions contained 130 mM-NaCl, 500 μM-EDTA, 100 μM-EGTA, 10 mM-Tris (pH 7·6), with added $MgCl_2$ or $CaCl_2$. For the Mg^{2+} experiments, the total added and the expected free magnesium concentrations were, respectively (M): $2{\cdot}40 \times 10^{-5}$, 10^{-7}; $1{\cdot}71 \times 10^{-4}$, 10^{-6}; $4{\cdot}30 \times 10^{-4}$, 10^{-5}; $5{\cdot}90 \times 10^{-4}$, 10^{-4}; $1{\cdot}50 \times 10^{-3}$, 10^{-3}; and $1{\cdot}05 \times 10^{-2}$, 10^{-2}. For the Ca^{2+} experiments, the corresponding total added and the expected free Ca^{2+} concentrations were (M): $5{\cdot}30 \times 10^{-4}$, 10^{-7}; $5{\cdot}93 \times 10^{-4}$, 10^{-6}; $6{\cdot}09 \times 10^{-4}$, 10^{-5}; $7{\cdot}00 \times 10^{-4}$, 10^{-4}; $1{\cdot}60 \times 10^{-3}$, 10^{-3}; and $1{\cdot}06 \times 10^{-2}$, 10^{-2}.

Excised-patch and whole-cell voltages were corrected for changes in the liquid junction potential between the bath and the bath reference electrode, a small 130 mM-NaCl–agar bridge that contacted a chlorided silver pellet. Using the method described by Baylor & Nunn (1986), the junction potentials between bath and bridge were measured as +3 (500 mM-NaCl in bath), −5 (50 mM-NaCl), −8 (25 mM-NaCl), −10 (15 mM-NaCl), −14 (5 mM-NaCl), −11 (5 mM-$MgCl_2$), and +5·5 mV (86·7 mM-$MgCl_2$). With a Ringer solution–agar bridge and the pseudo-intracellular solution in the bath, the measured junction potential was −10·4 mV.

Modelling

Theoretical excised-patch currents were calculated from the channel model shown in Fig. 1, assuming parameters for the energy profile, a number of channels in the patch, and particular ionic concentrations. A computer program used eqns (1), (2) and (6)–(9) (with similar expressions for divalent cations) and eqns (10)–(12) to calculate at each desired voltage the values for the rate constants k, probabilities P, fluxes F and, finally, the currents.

The distance and free energy parameters in the model of Fig. 1 were varied in an attempt to find a single set of parameters that best fitted all the results. The fitting was constrained by assuming that distance parameters d_i, d_w and d_o in Fig. 1 were the same for all species of ion. In fitting results from a given patch, a fixed number of channels, n, was assumed. The value of n used to fit current–voltage relations in symmetrical 130 mM-Na^+, low divalent solutions was constrained by the amplitude of the single-channel current observed under these conditions (Zimmerman & Baylor, 1986).

THEORY

This section presents equations used to describe ionic movements through the channel. The model is based on Eyring rate theory (see Hille, 1984) and is similar to that used previously by others (e.g. Hille, 1975; Lewis & Stevens, 1979). Treatment is restricted to the steady-state fluxes of Na^+, Ca^{2+} and Mg^{2+} through channels that are activated by a saturating concentration of cyclic GMP. Because only one divalent cation was usually present at a time, and because the model treats Ca^{2+} and Mg^{2+} as interchangeable (with suitable change of parameters), Ca^{2+} is not considered explicitly in the exposition below.

Suppose that as a cation passes through an open channel its relative energy varies with the fractional distance through the transmembrane electric field as shown in Fig. 1. Here a single energy well (ionic binding site) is flanked by two energy barriers, which represent restrictions on the ability of ions to reach and leave the binding site. For simplicity the barriers and the well are assumed to lie within the transmembrane electric field at fixed positions which are independent of the nature of the permeating ion. The barrier heights and well depth, however, depend on the nature of the cation and have characteristic free energies. We assume that only one cation can occupy the well at any given time.

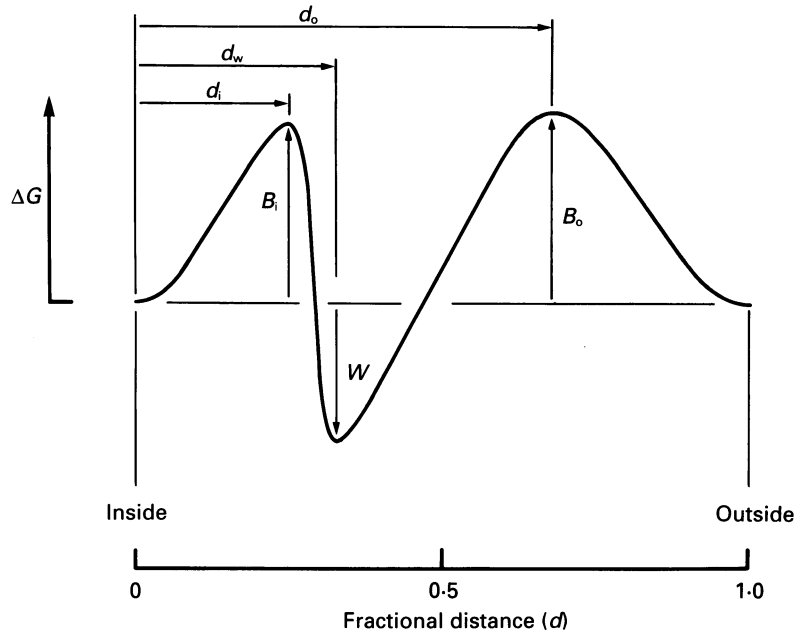

Fig. 1. Energy profile of barrier model for cation movements through the cyclic GMP-activated channel. Abscissa: fractional distance d through the transmembrane voltage field within the channel, measured from the inner (cytoplasmic) end. Ordinate: free energy difference (ΔG) between ions at the mouth of the channel and at positions plotted on the abscissa; convention for zero free energy difference described in text. Barrier and well positions are denoted by d_o, d_i and d_w; barrier and well energies are denoted by B_o, B_i and W. In the calculations in the text the distance parameters were: $d_i = 0{\cdot}25$, $d_w = 0{\cdot}33$, $d_o = 0{\cdot}68$, while the energy parameters were (units of RT, where R is the gas law constant and T is absolute temperature):

	B_i	W	B_o
Na^+	2·0	−9·3	3·8
Ca^{2+}	4·5	−19·1	2·0
Mg^{2+}	3·7	−17·1	4·4

Permeation of ions through the open channel can be represented as follows. For Na^+,

$$X + Na_o^+ \underset{k_3}{\overset{'k_1}{\rightleftharpoons}} NaX \underset{'k_4}{\overset{k_2}{\rightleftharpoons}} X + Na_i^+,$$

where X stands for the empty state of the channel, NaX denotes the state in which Na is bound, Na_o^+ and Na_i^+ represent sodium in the external and internal solutions respectively, and the ks are rate constants which depend on the energy profile and the membrane potential as described below. Rate constants $'k_1$ and $'k_4$ have dimensions $s^{-1}\ M^{-1}$, while rate constants k_2 and k_3 have dimensions s^{-1}. Similarly, permeation by Mg^{2+} is

$$X + Mg_o^{2+} \underset{k_7}{\overset{'k_5}{\rightleftharpoons}} MgX \underset{'k_8}{\overset{k_6}{\rightleftharpoons}} X + Mg_i^{2+}.$$

Let P_{Na}, P_{Mg} and P_X denote the respective probabilities that the well in an open channel is occupied by Na^+, occupied by Mg^{2+}, and empty. Then

$$dP_{Na}/dt = P_X('k_1[Na^+]_o + 'k_4[Na^+]_i) - P_{Na}(k_2 + k_3)$$

and

$$dP_{Mg}/dt = P_X('k_5[Mg^{2+}]_o + 'k_8[Mg^{2+}]_i) - P_{Mg}(k_6 + k_7),$$

where the terms in square brackets denote ionic concentrations (strictly activities). In the steady state the time derivatives in these expressions are zero, and the net Na^+ and Mg^{2+} effluxes F_{Na} and F_{Mg} through the channel are

$$F_{Na} = 'k_4 P_X[Na^+]_i - k_2 P_{Na} \quad (1)$$

and

$$F_{Mg} = 'k_8 P_X[Mg^{2+}]_i - k_6 P_{Mg}. \quad (2)$$

If the channel is open all of the time, the probabilities P_X, P_{Na}, and P_{Mg} depend on the ionic activities and the rate constants according to the expressions:

$$P_X = 1 - P_{Na} - P_{Mg}, \quad (3)$$

$$P_{Na} = (NK_{Mg})/(NK_{Mg} + K_{Mg}K_{Na} + MK_{Na}) \quad (4)$$

and

$$P_{Mg} = (MK_{Na})/(NK_{Mg} + K_{Mg}K_{Na} + MK_{Na}). \quad (5)$$

In these expressions,

$$N = 'k_1[Na^+]_o + 'k_4[Na^+]_i,$$

$$M = 'k_5[Mg^{2+}]_o + 'k_8[Mg^{2+}]_i,$$

$$K_{Na} = k_2 + k_3,$$

$$K_{Mg} = k_6 + k_7.$$

Ionic fluxes calculated by eqns (1) and (2) were converted to electrical currents by multiplying by the factor zF/N_A where z is the ionic valence, F is Faraday's constant, and N_A is Avogadro's number. The total patch current is the sum of the Na^+ and Mg^{2+} currents through a single channel multiplied by the number of channels in the patch.

The ks in eqns (1)–(5) depend on the parameters of the energy profile and the membrane potential V according to:

$$'k_1 = b \exp(-B_o) \exp(-(1-d_o)VzF/RT), \quad (6)$$

$$k_2 = (kT/h) \exp(-(B_i - W)) \exp(-(d_w - d_i)VzF/RT), \quad (7)$$

$$k_3 = (kT/h) \exp(-(B_o - W)) \exp((d_o - d_w)VzF/RT), \quad (8)$$

and

$$'k_4 = b \exp(-B_i) \exp(d_i VzF/RT). \quad (9)$$

Constant b in eqns (6) and (9) is the bimolecular rate constant, taken as 2×10^9 M^{-1} s^{-1} (Fersht, 1985); the product of b and the appropriate ionic concentration is the frequency at which ions reach the mouth of a channel. Constant k is the Boltzman constant, h is Planck's constant, T is the absolute temperature, z is the valency of the ion and R is the gas law constant. V is the membrane voltage (internal potential minus external potential). The barrier and well positions (d_o, d_i and d_w) and energies (B_o, B_i and W) are as defined in Fig. 1. Similar expressions, with $z = 2$ and appropriate barrier and well energies, give the divalent rate constants $'k_5$, k_6, k_7 and $'k_8$.

Results presented elsewhere (Karpen, Zimmerman, Stryer & Baylor, 1988*a*) suggest that a fully-liganded channel undergoes rapid open–closed transitions, and

that the equilibrium between open and closed channels is slightly voltage dependent. At the saturating concentrations of cyclic GMP used here the voltage dependence of the open probability appears to be quite weak. Nevertheless, by favouring the open state, positive potentials will slightly increase outward currents. The quantitative effect that the voltage dependence of channel activation will have on steady-state current–voltage relations depends on how gating and permeation interact. In attempting to allow for the voltage dependence of gating, we have adopted the simplest assumption, that the processes are independent. This implies that the channel opens and closes in the same way whether the well is empty or occupied and that the fractional occupancy of the well is identical for the open and closed states. The open–closed equilibrium between fully-liganded channels may then be represented

$$\text{closed} \underset{\beta}{\overset{\alpha}{\rightleftharpoons}} \text{open},$$

where the rate constants α and β are voltage dependent. Now in the steady state

$$(P_{Mg}+P_{Na}+P_X)/P_C = \alpha/\beta$$

and

$$P_{Mg}+P_{Na}+P_X+P_C = 1,$$

where P_C is the probability that the channel is closed, all closed states being treated as equivalent. The probabilities that open channels are occupied or empty will be given by

$$P_X = a - P_{Mg} - P_{Na}, \tag{10}$$

and

$$P_{Na} = aNK_{Mg}/(NK_{Mg}+K_{Mg}K_{Na}+MK_{Na}) \tag{11}$$

in which

$$P_{Mg} = aMK_{Na}/(NK_{Mg}+K_{Mg}K_{Na}+MK_{Na}), \tag{12}$$

$$a = \alpha/(\alpha+\beta).$$

Rate constant α was taken as $1{\cdot}44 \times 10^4\ s^{-1}$, and the value of β at voltage V (mV) was taken as (Karpen *et al.* 1988*a*)

$$\beta = (3{\cdot}45 \times 10^3\ s^{-1}) \exp(-V/123\ mV).$$

The zero energy on the ordinate in Fig. 1 is different than that in the model of Hille (1975). He refers ionic free energies to those in a 1 M standard bulk solution and uses $kT\,h^{-1}\,M^{-1}$ as the pre-exponential term in the expressions for rate constants $'k_1$, $'k_4$, $'k_5$ and $'k_8$. We have taken the zero energy as that of a mole of ions at the mouth of the channel. Barrier and well energies on the two scales are related by $E = E' + 8{\cdot}0$, where E' is the energy here and E is that on Hille's (1975) scale. A well of $-18{\cdot}5\ RT$ units here corresponds to one of $-10{\cdot}5$ on his scale. Lewis & Stevens (1979) take the value of b as $10^{11}\ M^{-1}\ s^{-1}$, so that their energy scale has a value of zero at $\ln(2 \times 10^9/1 \times 10^{11}) = -3{\cdot}9$ on our scale. It should be noted that the values for the transition rate constants in the model are independent of the convention adopted for the zero free energy.

RESULTS

Relative permeabilities to Na^+ and Cl^-

Figure 2*A* shows how the cyclic GMP-activated current depended on the concentration of NaCl in the solution bathing the inner surface of an excised patch. Divalent cations were present at very low concentrations in the bath and pipette

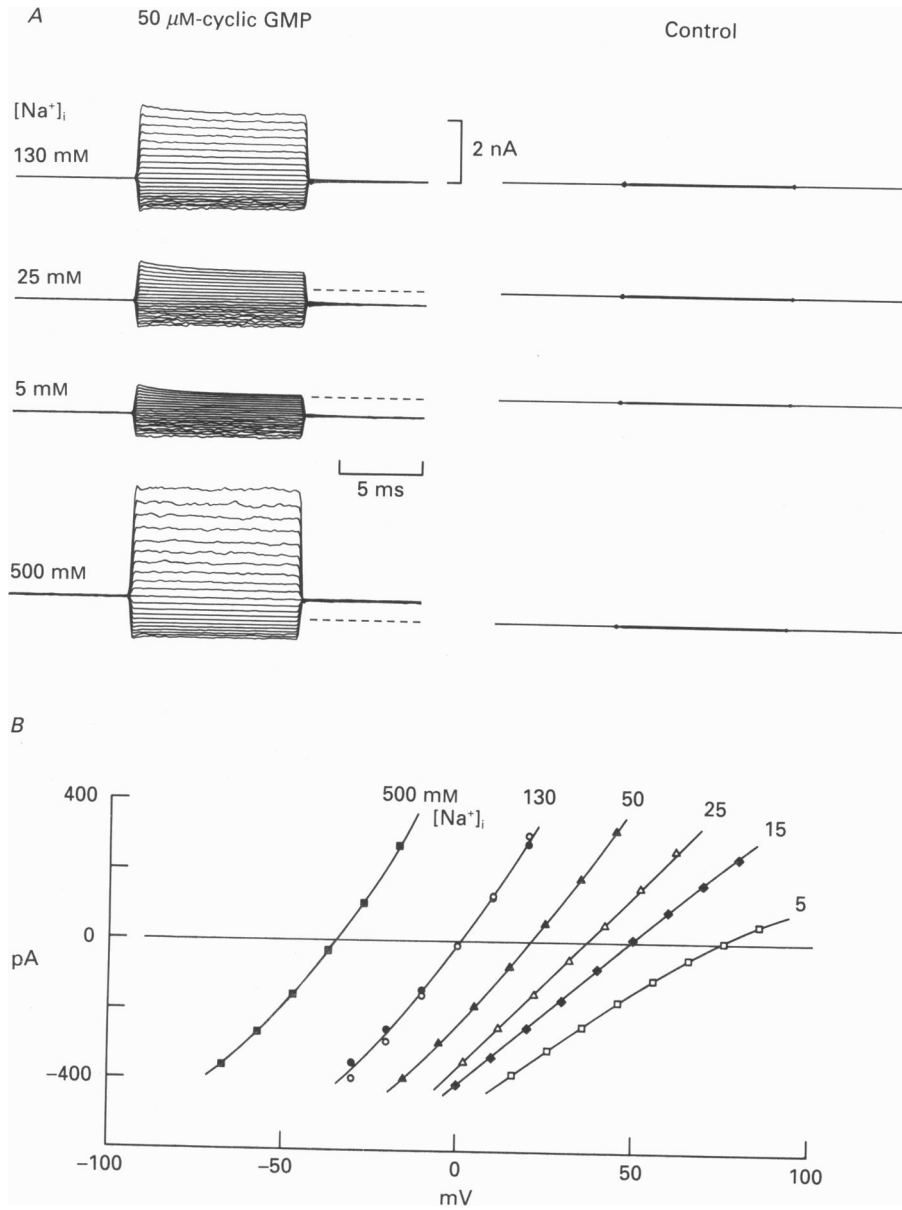

Fig. 2. *A*, effect of changing internal NaCl concentration on cyclic GMP-induced patch currents. Patch voltage was held at 0 mV (not corrected for junction potential change) and switched from −100 to +100 mV in 10 mV steps. Families on the left were obtained with 50 μM-cyclic GMP in the chamber, families on the right without cyclic GMP. Dashed lines show zero current level. Patch pipette contained the low divalent solution with 130 mM-NaCl. The internal (bath) solution contained the indicated concentration of NaCl. Sucrose was added to keep the osmolarity of the internal solution constant when the concentration of NaCl was lowered; at 500 mM-NaCl there was an uncompensated increase in osmolarity. Bandwidth 0–2 kHz (8-pole Bessel low-pass filter), sampling rate 10 kHz. Pipette resistance before sealing 4·7 MΩ; seal resistance 11 GΩ initially, 6 GΩ at end. Temperature 22·5 °C. *B*, plot of cyclic GMP-induced difference current as a function of patch voltage, with voltage corrected for junction potentials. Average currents were

solutions (none added, 20 μM-EDTA). The currents in each panel were evoked by a series of voltage pulses with amplitudes varying between -100 and $+100$ mV. Comparison of the currents on the left, recorded in the presence of cyclic GMP, with those on the right, recorded without cyclic GMP, indicates that nearly all the current was cyclic GMP activated. Changing the internal NaCl concentration changed the reversal potential for the cyclic GMP-activated current and the size of the outward current at positive potentials. Figure 2*B* shows how the reversal potentials were determined. Steady-state patch current is plotted against corrected membrane voltage. Lowering the internal concentration of NaCl shifted the reversal potential in the positive direction, while raising the concentration made the reversal potential more negative. These results are expected if Na^+ passes through the channel more easily than Cl^-.

Figure 3 summarizes results from similar experiments on four patches. The mean reversal potentials (points) are not far from the dashed line, which is the Na^+ equilibrium potential E_{Na} calculated from the Nernst equation. One explanation of the systematic deviation at low Na^+ activities would be that the channel is somewhat permeable to chloride. The continuous line was calculated from the Goldman–Hodgkin–Katz voltage equation, on this assumption. According to this equation (e.g. Hille, 1984, p. 233), the reversal potential V_r of the current across a conductance with a ratio p of permeabilities for chloride and sodium ions is given by

$$V_r = (RT/F) \ln\{([Na^+]_o + p[Cl^-]_i)/([Na^+]_i + p[Cl^-]_o)\}.$$

The continuous line in Fig. 3 was drawn assuming that $p = 0{\cdot}020$. Measurements by Fesenko, Kolesnikov & Lyubarsky (1986) at a twofold concentration gradient of NaCl are consistent with $p = 0{\cdot}028$. The Goldman–Hodgkin–Katz equation, which assumes independence and a constant field, may not strictly apply but is useful as an empirical description.

This Cl^-–Na^+ permeability ratio is probably an upper limit. Thus at low internal Na^+ concentrations there was a steady inward current at the nominal 0 mV holding voltage. This current will elevate the Na^+ concentration at the inner surface of the patch, where a slab of adhering material hinders ionic diffusion (Zimmerman, Karpen & Baylor, 1988). At the end of the pulse, when the currents were measured, the Na^+ concentration at the inner patch surface may still have been slightly elevated, giving a reversal potential less positive than the true value. Indeed the slight droop in the outward currents in Fig. 2*A* results from a reduction in the driving force on the outward current due to depletion of Na^+ at the inner surface of the patch (Zimmerman *et al.* 1988). Such ion accumulation/depletion effects are ignored elsewhere in this paper because they are relatively small.

It seems unlikely that the deviation from Nernstian behaviour in Fig. 3 results from proton movements through the channel. Using the Goldman–Hodgkin–Katz equation to fit the results on this assumption required a proton permeability about 10^5 times larger than the Na^+ permeability.

---

measured over a 2 ms window beginning 8 ms after the start of the pulse. Reversal potentials were estimated as $-34{\cdot}8$, $+1{\cdot}0$, $+20{\cdot}3$, $+36{\cdot}3$, $+49{\cdot}3$ and $+75{\cdot}0$ mV respectively (left to right); smooth curves for interpolation were drawn by eye. Experiment began and ended with runs at 130 mM (○, ●).

Dependence of outward current on internal Na^+ concentration

Several lines of evidence suggest that currents through the cyclic GMP-gated channel do not obey the independence principle (Hodgkin & Huxley, 1952). For example, divalent cations, which permeate the channel, strongly reduce the size of

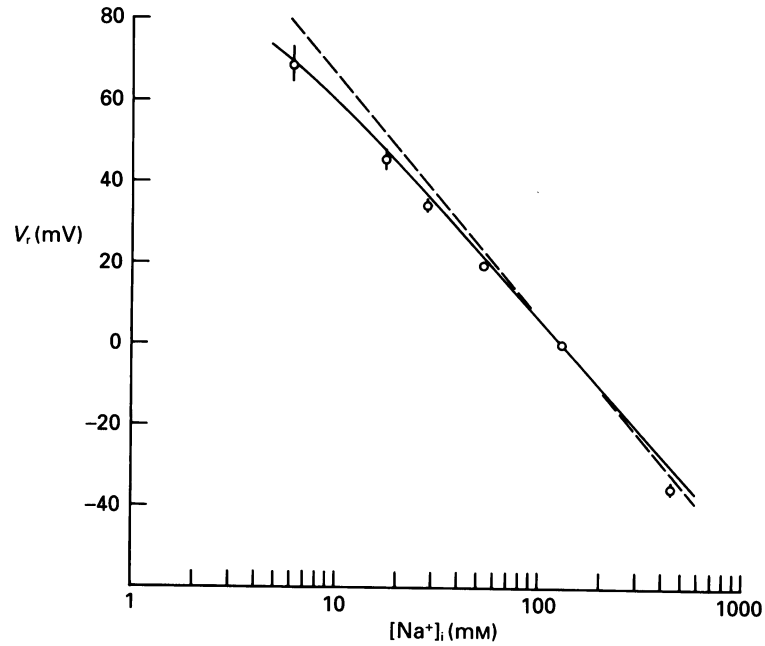

Fig. 3. Dependence of reversal potential of cyclic GMP-activated patch current on the internal Na^+ concentration. Collected results from four patches, including that of Fig. 2. External NaCl concentration 130 mM, low divalent solution. Points are the means of four determinations (only three for 500 mM point), bars the standard deviation of the measurements. Concentrations have been multiplied by the activity ratio a_x/a_{130} where a_x is the activity at concentration x and a_{130} is the activity at 130 mM. Activities were obtained from tables III and V in MacInnes (1961), pp. 164 and 167. Interrupted line has a slope of 59 mV decade^{-1} passing through $V = 0$ at 130 mM, as expected if only Na^+ permeates the channel under these conditions. Continuous line calculated from Goldman–Hodgkin–Katz equation with the chloride–sodium permeability ratio = 0·020. Currents at +100 mV with $[Na^+]_i$ = 130 mM ranged between 220 and 2609 pA. Internal cyclic GMP concentration 50 μM, solutions as in the experiment of Fig. 2.

Na^+ currents through it (reviewed by Yau & Baylor, 1989). Furman & Tanaka (1990) and Menini (1990) reported violations of independence even in solutions containing only monovalent cations. Figure 4 confirms the violation of independence in sodium solutions without divalent cations. The points show steady-state current–voltage relations for the cyclic GMP-induced currents of the patch of Fig. 2. If Na^+ movements through the channel obeyed the independence principle, at a membrane potential of 0 mV the Na^+ current should vary linearly with the Na^+ concentration difference across the membrane. In Fig. 4, the current at 0 mV with 5 mM internal Na^+ (130 mM external Na^+) was −0·49 nA. Assuming independence, a current of 1·45 nA is expected at $[Na^+]_i$ = 500 mM, compared to 0·58 nA actually observed. In

three patches studied in this way the ratio of the current observed to that expected from independence was 0·406 (mean, range 0·400–0·415). The failure to obey independence suggests that the channel contains a bottleneck that limits the flow of ions through it. The magnitude of the deviation from independence is similar to that

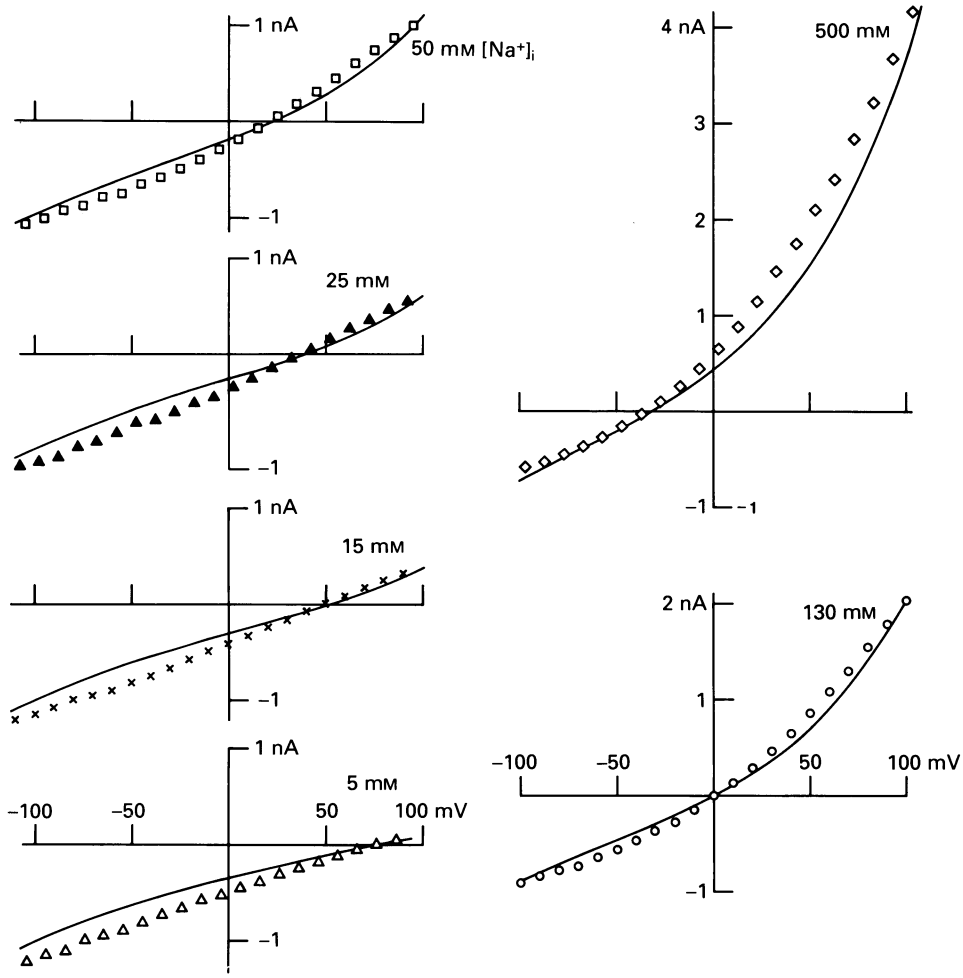

Fig. 4. Steady-state current–voltage relations of cyclic GMP-activated patch conductance at different internal Na^+ concentrations, with 130 mM-NaCl in the patch pipette. Results from the patch of Fig. 2. Ordinate is cyclic GMP-activated current, measured over a window 8–10 ms after voltage was switched from the holding potential (nominally 0 mV). Voltages were corrected for junction potential changes. Continuous curves were calculated from the model described in the text, using the appropriate ionic activities and assuming 765 channels in the patch. Points at $[Na^+]_i = 130$ mM are means from runs at the beginning and end of the experiment; the individual values differed by less than 10%.

predicted by the one-site model described above (continuous curves). Much larger deviations from independence are seen in K^+ and Ca^{2+} channels, which appear to have multiple ion occupancy (see e.g. Hille, 1984).

The collected excised-patch results in Fig. 5 confirm that the outward current did

not grown linearly with increasing internal Na^+ concentration. Current at +90 mV is plotted as a function of internal Na^+ activity on double log scales. Although the current did not completely saturate, it failed to grow linearly with increasing Na^+ activity. Unfortunately currents could not be measured at higher internal Na^+

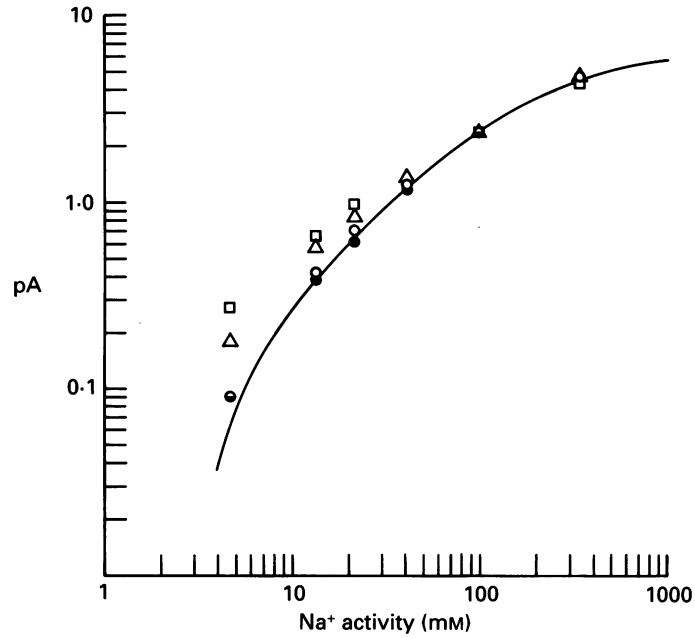

Fig. 5. Dependence of the normalized outward current at +90 mV on internal Na^+ activity. Collected results from the four patches of Fig. 3. Currents from each patch were measured over a time window 8–10 ms after the voltage was switched and were normalized by the estimated number, n, of channels in the patch; n was obtained by taking the single-channel current to be 2·34 pA at an internal Na^+ activity of 99·2 mM. Continuous curve calculated from the model described in the text, using a Na^+ activity in the pipette of 99·2 mM (concentration 130 mM). Saturating current for the model was 6·65 pA. For each patch, the raw current at 99·2 mM-Na^+ activity and the estimated number of channels were: ○, 1790 pA, 765 (patch of Figs 2 and 4); ●, 2319 pA, 991; △, 182 pA, 78; □, 361 pA, 154.

concentrations because patches did not tolerate such high concentrations. The dependence of current on Na^+ is consistent with the idea that a Na^+ ion passing through the channel bound to a site that was occupied half the time when the internal Na^+ activity was about 180 mM. The continuous curve in Fig. 5 was calculated from the model described in the theoretical section, with parameters given in the legend to Fig. 1. The fit is satisfactory except at small Na^+ activities, where the currents from two patches lie above the theoretical relation. This deviation is consistent with the ion accumulation effect discussed above and/or a finite permeability to ions other than Na^+.

Form of current–voltage relations in Na^+ solutions

In Fig. 4 the experimental current–voltage relations at $[Na^+]_i$'s of 50, 130 and 500 mM rectify outwardly. At a $[Na^+]_i$ of 15 mM there was little outward rectification, and at 5 mM the current–voltage relation was almost linear. The continuous curves

in Fig. 4 were calculated from the model of Fig. 1. Although the curves provide a reasonable fit they are somewhat less linear then the measured relations. This discrepancy is particularly marked at the lowest and highest internal Na^+ concentrations. In the model adopted here, most of the outward rectification in Fig. 4

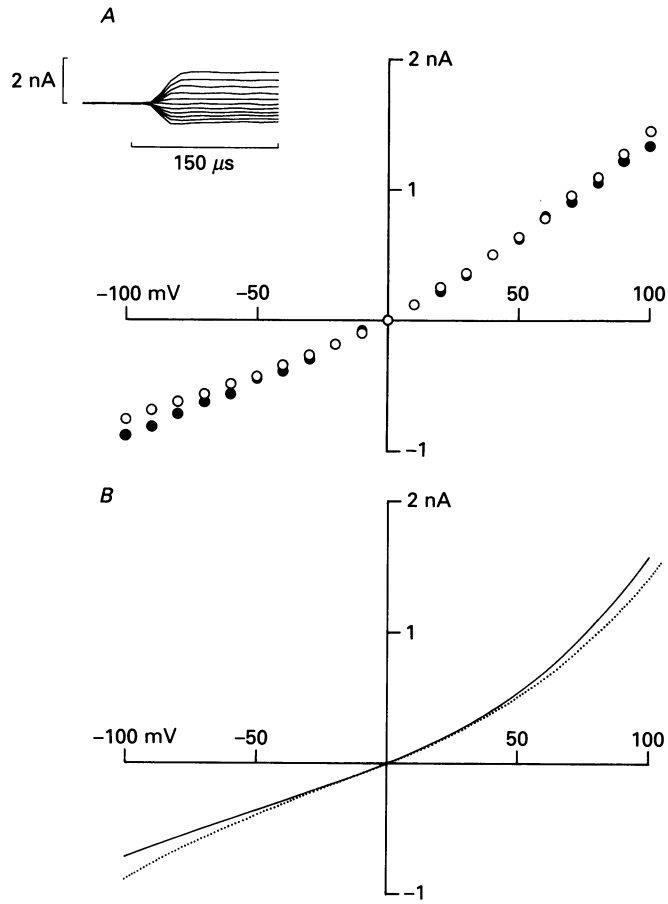

Fig. 6. Current–voltage relations of the cyclic GMP-activated patch conductance in symmetrical 130 mM-NaCl low divalent solutions, at fixed early and late times after changing the voltage. *A*, experimental relations measured at 50 μs (●) and 1 ms (○) after switching the voltage from 0 mV. Each point is the average difference current (current in presence of 200 μM-cyclic GMP − current without cyclic GMP) from four interleaved trials on the same patch. Currents were low-pass filtered at 20 kHz (−3 dB point, 8-pole Bessel) and sampled at 100 kHz. Solutions contained 50 μM-EDTA. Pipette was Sylgard coated. Inset, rising phase of average difference currents for voltage jumps of −100 to +100 in steps of 20 mV. The voltage was switched at the left edge of the time scale bar. *B*, current–voltage relations calculated from the channel model, neglecting voltage-dependent gating of the channel (dotted curve), or allowing for it as described in the text (continuous curve). For the calculations the patch was assumed to contain 570 channels. Ratios of currents at +100 mV and −100 mV were: 1·52 (●), 1·92 (○), 1·59 (dotted), 2·22 (continuous).

derives from the asymmetry in the channel's barrier–well structure. A smaller contribution is made by the voltage dependence of the open–closed equilibrium of the channel, with depolarization favouring the open state (see Karpen *et al.* 1988*a*). All patches showed outward rectification when studied in symmetrical solutions containing only monovalent cations. For eighteen patches in symmetrical 130 mM-Na^+ solutions without divalent cations the ratio of the currents at +100 and −100 mV was 2·0 ± 0·4 (mean ± standard deviation).

Figure 6*A* presents a test of the notion that the outward rectification in symmetrical Na^+ solution indeed derived mainly from the voltage dependence of sodium permeation. The aim was to compare current–voltage relations measured in excised patches at two times: (a) just after switching the voltage, before the channels' open–closed equilibrium could change, and (b) in the steady state. The filled circles show currents measured 50 μs after the onset of the voltage pulse, the open circles the currents at 1 ms. We attribute the rectification in the early relation to the voltage dependence of Na^+ permeation and the slight additional rectification at 1 ms to voltage dependence of the fully-liganded channel's open probability, depolarization favouring the open state (see Karpen *et al.* 1988*a*).

The inset in Fig. 6*A* shows the time course of the currents and the relaxations that converted the current–voltage relation from the early to the late form. About 50 μs after switching the voltage, the current at −100 mV began to fall, while that at +100 mV continued to rise, presumably as channels closed and opened, respectively. The earliest time at which useful measurements could be made was 50 μs after switching the voltage since simulations showed that currents at prior times would be artifactually linearized by the finite rise time of the voltage step (about 10 μs) and the response time and lag (25 μs) of the 20 kHz low-pass filter. Thus, if the patch voltage had not reached its full amplitude, currents measured at the time would show less rectification. The curves in Fig. 6*B* were calculated from the channel model. The dotted line was obtained assuming voltage-dependent permeation without voltage-dependent gating, while the continuous line was calculated allowing for the voltage dependence of gating, on the assumption that permeation and gating are independent (see Theory section). Results similar to those of Fig. 6*A* were obtained in experiments on six other patches. The tentative conclusion is that the form of the steady-state relation was mainly determined by the voltage dependence of ion permeation, with the voltage dependence of the channel's open probability making a small additional contribution. In principle measuring the current–voltage relation of a single open channel could be used to test this conclusion, but such measurements are difficult because of the very rapid open–closed transitions in the fully-liganded channel.

Block of Na^+ current by internal divalent cations

Adding Mg^{2+} or Ca^{2+} to the internal solution strongly reduced the cyclic GMP-activated current. In eighteen experiments without internal divalent cations the current at +100 mV was 1949 ± 1466 pA (mean ± S.D.) compared with 163 ± 157 pA when 1–7·5 mM-Mg^{2+} or Ca^{2+} was added to the isotonic Na^+ solution bathing the internal surface of the patch. In five experiments in which only Mg^{2+} or Ca^{2+} was present, at concentrations of 5–87·5 mM, the outward current at +100 mV was even smaller, 27 ± 29 pA.

Figure 7 shows collected results from excised patch experiments to determine the concentration dependence of Mg^{2+} block of the Na^+ current. The ordinate is the cyclic GMP-activated chord conductance, normalized to the estimated mean value for an unblocked single channel, while the abscissa is the $[Mg^{2+}]_i$ on a log scale. The external

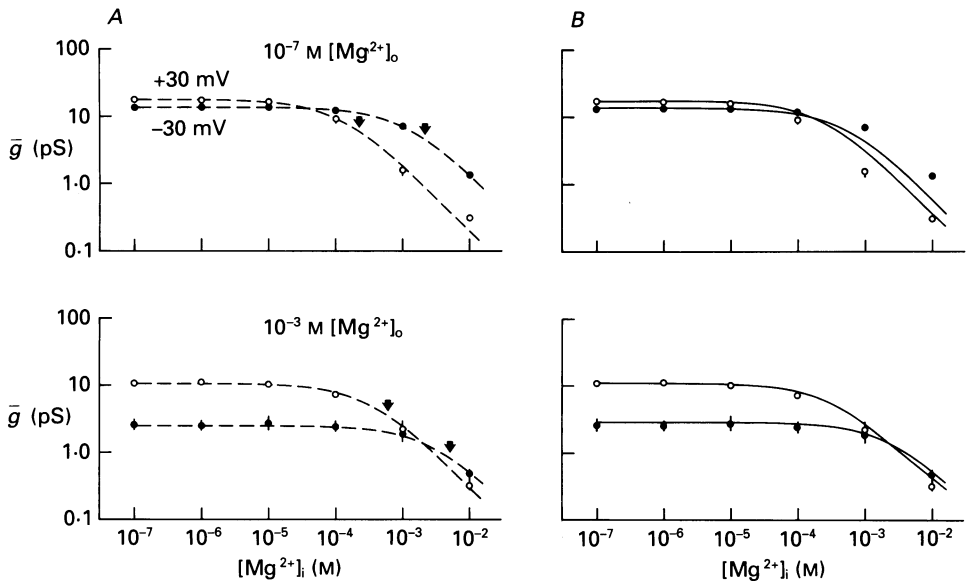

Fig. 7. Block of the cyclic GMP-activated conductance by $[Mg^{2+}]_i$. ○ and ● show normalized steady-state conductances at +30 and −30 mV respectively. Results from each patch have been scaled to the estimated mean single-channel conductance of an unblocked channel ($\bar{g}$). The upper and lower panels each present results from three different patches. The points are averages and the vertical lines show the range of the measurements. *A*, results fitted empirically with titration curves. In the upper panel the $[Mg^{2+}]_o$ was 10^{-7} M and the apparent dissociation constant for block by internal Mg^{2+} was 220 μM at +30 mV and 2·1 mM at −30 mV. Number of channels, *n*, for the patches was taken as 49, 370, and 1017. Leakage resistances were 2·5, 7, and 10 GΩ. In the lower panel the $[Mg^{2+}]_o$ was 10^{-3} M and the apparent dissociation constants were 600 μM at +30 mV and 5·0 mM at −30 mV; *n* for the three patches were taken as 57, 600, and 636. Leakage resistances were 4·3, 10 and 12 GΩ. *B*, same results compared with the prediction of the channel model. Conductances were determined by dividing the cyclic GMP-activated current, measured over a window 8–10 ms after switching the voltage from 0 mV, by the patch voltage. Solutions as described in Methods.

and internal solutions contained 130 mM-NaCl, so that Na^+ was the dominant current carrier. Measurements were made at +30 mV (○) and at −30 mV (●). In Fig. 7*A* the normalized conductances have been fitted with simple titration curves (dashed curves) while Fig. 7*B* compares the same results to the predictions of the channel model.

For the experiment in the upper panel of Fig. 7*A* the $[Mg^{2+}]_o$ was 0·1 μM. The apparent dissociation constant for internal Mg^{2+} was estimated as 220 μM at +30 mV and as 2·1 mM at −30 mV. The voltage dependence of the dissociation constant suggests that Mg^{2+} binds to a site that lies within the transmembrane

electric field: at a given concentration of internal Mg^{2+}, depolarization increases the fractional occupancy of the binding site.

If both external and internal Mg^{2+} ions block Na^+ current by combining with the same site in the channel, the apparent dissociation constant for block from the inside

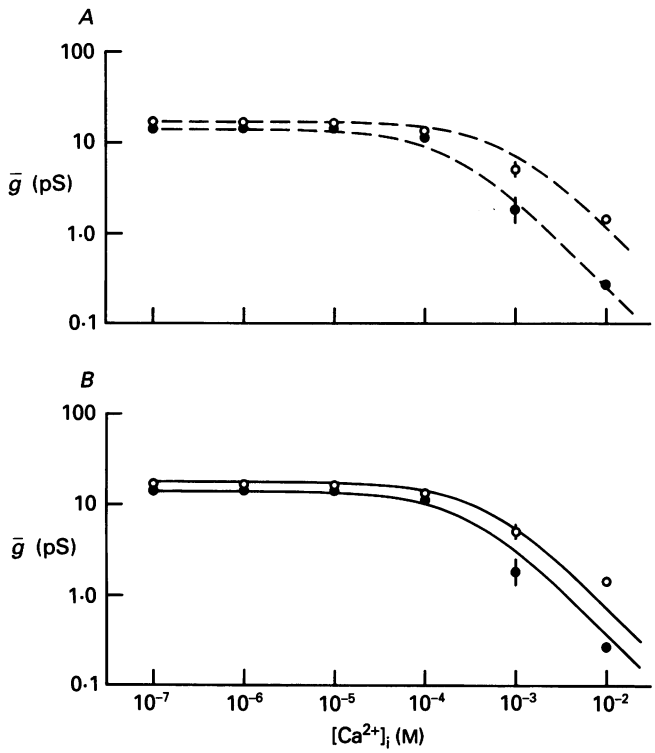

Fig. 8. Dependence of the normalized steady-state cyclic GMP-activated conductance on $[Ca^{2+}]_i$, with very low concentrations of external divalent cations. Collected results from three patches with each measurement scaled to the estimated mean single-channel conductance of an unblocked channel. *A*, ○ and ● circles show mean values at +30 and −30 mV respectively; vertical lines give range of values. Dashed lines are titration curves fitted to the points by eye. The apparent dissociation constants of the curves were 400 μM (−30 mV) and 1·4 mM (+30 mV). Numbers of channels and leakage resistances were: 1300, 4·3 GΩ; 860, 10 GΩ; 980, 12 GΩ. The cyclic GMP-activated currents were measured 8–10 ms after the voltage was switched from 0 mV and were converted to conductance by dividing by the voltage. Solutions as described in Methods. *B*, same experimental results as in *A*. Continuous curves drawn according to the model in the text.

should increase when the channel is already partially blocked by external Mg^{2+}. The experiments in the lower panel of Fig. 7*A* test this prediction. The conductance was titrated with internal Mg^{2+} in the presence of 1 mM external Mg^{2+}. At low internal Mg^{2+} the conductance at −30 mV was smaller than that at +30 mV because of the voltage dependence of block by external Mg^{2+}. The experimental results again were fitted satisfactorily by simple titration curves, but the apparent dissociation constants were 0·600 (+30 mV) and 5·0 mM (−30 mV). These values are significantly higher than those observed at low $[Mg^{2+}]_o$, as expected if block indeed occurred at a

single site within the channel. For one-site block, external Mg^{2+} should increase the dissociation constant by the same factor by which it blocks the channel at low internal Mg^{2+}. The results roughly agree with this notion.

Figure 7*B* compares the results with the predictions of the model. At low $[Mg^{2+}]_o$ the experimentally observed block was more voltage dependent than block in the

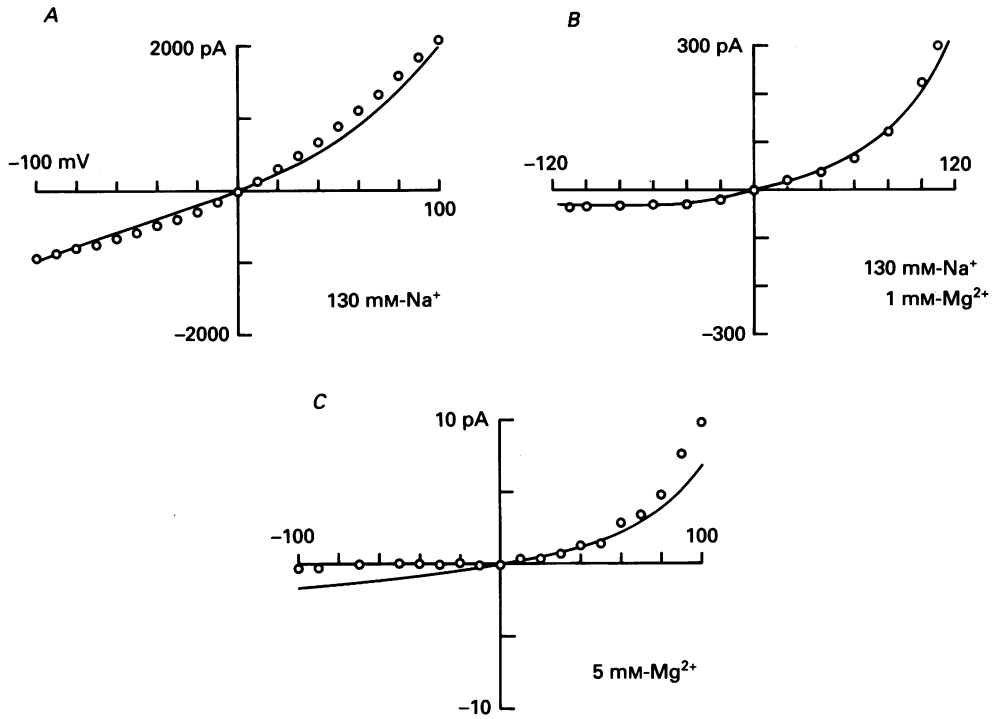

Fig. 9. Steady-state current–voltage relations for the cyclic GMP-gated conductance from three patches exposed to symmetrical solutions with and without Mg^{2+}. Ordinate is average current activated by 50 μM-cyclic GMP measured in a window 8–10 ms after voltage was switched. Continuous curves drawn according to model in text. *A*, relation with symmetrical NaCl, at 130 mM, same experiment as in Fig. 2. *B*, relation for symmetrical solutions consisting of a mixture of 130 mM-NaCl and 1 mM-$MgCl_2$. Currents were activated by 200 μM-cyclic GMP. *C*, relation for symmetrical 5 mM-$MgCl_2$ solutions, no added NaCl, osmolarity balanced with sucrose. Bandwidth 0–200 Hz, 8-pole Bessel low-pass filter, sampling interval 100 μs.

model. Nevertheless it is satisfactory that the theoretical curves cross over each other as the experimental curves do. The fit to the results with 1 mM external Mg^{2+} is reasonable.

Figure 8 presents excised-patch results on the block of Na^+ currents by internal Ca^{2+}. In Fig. 8*A* the normalized Na^+ conductances are fitted by titration curves with dissociation constants of 0·4 mM (results at −30 mV, ●) and 1·4 mM (+30 mV, ○). Depolarization reduced the efficiency of block, so that the voltage dependence of block by internal Ca^{2+} was opposite to that of block by internal Mg^{2+}. Figure 8*B* compares the results with the prediction of the model. The fit is reasonable, although the theoretical curves have too little voltage dependence. In the model, the difference

in the voltage dependence of block by Ca^{2+} and Mg^{2+} arises from their different energy profiles for permeation. For Mg^{2+} the external barrier is higher than the internal barrier and depolarization favours occupancy of the well by internal Mg^{2+}. For Ca^{2+} the internal barrier is higher and depolarization decreases occupancy of the well by internal Ca^{2+}.

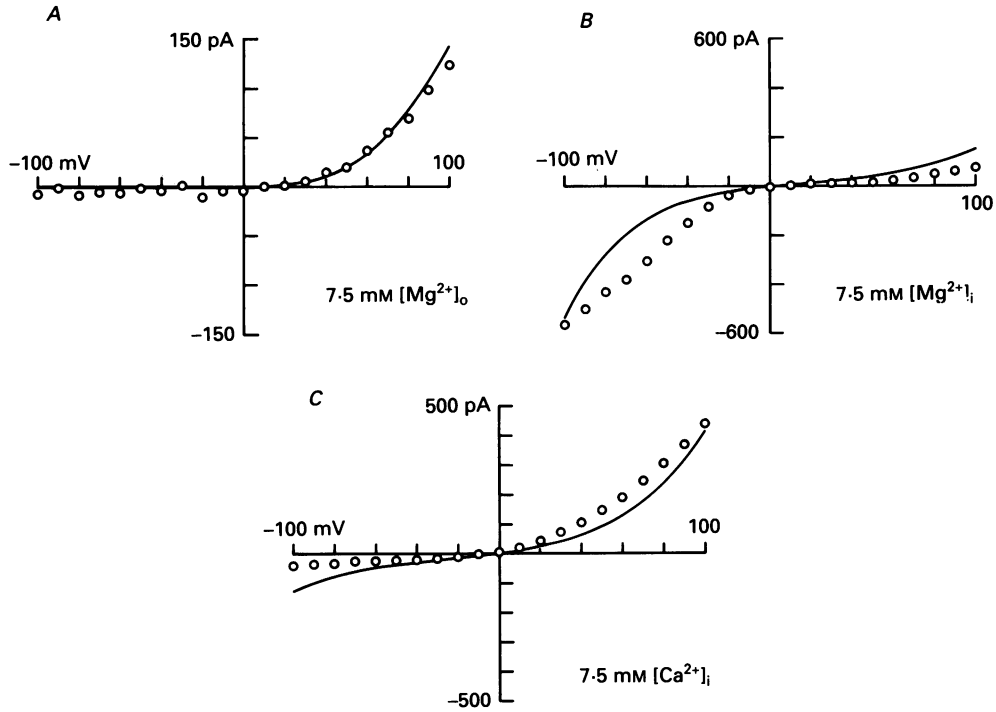

Fig. 10. Steady-state current–voltage relations for the cyclic GMP-gated conductance of patches in symmetrical 130 mM-NaCl with $MgCl_2$ or $CaCl_2$ added on only one side of the membrane. Ordinate is current activated by 200 μM-cyclic GMP, measured over a window 8–10 ms after voltage was switched. Continuous curves drawn according to model in text. *A*, outward rectification with 7·5 mM-$MgCl_2$ in the external solution. *B*, inward rectification with 7·5 mM-$MgCl_2$ in the internal solution. *C*, outward rectification with 7·5 mM-$CaCl_2$ in the external solution. Bandwidth 0–6000 Hz, sampling interval 20 μs.

Current–voltage relations with divalents present

Figure 9 compares current–voltage relations obtained from excised patches with symmetrical solutions containing 130 mM-NaCl (panel *A*), 130 mM-NaCl with 1 mM-$MgCl_2$ (panel *B*), and 5 mM-$MgCl_2$ (panel *C*). Addition of $MgCl_2$ to the NaCl solution increased the outward rectification of the cyclic GMP-induced current. In symmetrical $MgCl_2$ the outward rectification was more pronounced, and the inward current at negative voltages was very small. The fact that the rectification in $MgCl_2$ solutions was steeper than that in NaCl solutions provides independent evidence that a sizeable fraction of the channel's rectification results from the voltage dependence of ionic permeation at the channel. Thus, if rectification results from the voltage dependence of ion movements past energy barriers, divalent current carriers, which

feel the electric field more intensely, will give more rectification. Voltage-dependent changes in the channel's open probability would give similar rectification for monovalent and divalent cations. The continuous curves in Fig. 9, calculated from the model, provide reasonable fits to the experimental results.

Figure 10 illustrates current–voltage relations obtained from excised patches in symmetrical 130 mM-NaCl solutions to which $MgCl_2$ or $CaCl_2$ was added on only one side of the membrane. When 7·5 mM-$MgCl_2$ was present in the external solution there was strong outward rectification (e-fold in 18 mV), while with the same concentration of $MgCl_2$ in the internal solution the rectification was inward. These results suggest that hyperpolarization favours channel block by external Mg^{2+} while depolarization favours block by internal Mg^{2+}. As shown in panel *C*, adding 7·5 mM-$CaCl_2$ to the internal solution gave strong outward rectification, opposite to the inward rectification induced by internal $MgCl_2$. The curves were drawn according to the model.

Comparison of rectification in transducing rods with that in excised patches

Figure 11 compares current–voltage relations for the light-sensitive conductance in a transducing rod and the cyclic GMP-activated conductance of an excised patch exposed to the same ionic solutions (Ringer solution outside and the pseudo-intracellular solution at the inside surface). The current–voltage relation for the excised patch (lower panel) showed outward rectification that was somewhat more shallow (changing e-fold in 24–30 mV in three patches) than that of the light-sensitive conductance of the transducing rod (upper panel; e-fold in $17{\cdot}1 \pm 3{\cdot}4$ mV, mean ± S.D. for seven cells). The slight difference in degree of rectification may reflect a difference in the concentration of cyclic GMP (see Discussion). Measured reversal potentials for the light-sensitive and cyclic GMP-activated conductances were also similar: in eleven transducing rods, the reversal potential of the light-regulated conductance was $+7{\cdot}8 \pm 5{\cdot}7$ mV (mean ± S.D.), while the cyclic GMP-activated conductance in three patches studied with the same (approximately physiological) solutions had reversal potentials ranging from +7·6 to +12·6 mV. It was not feasible to simulate data obtained with these complex solutions, but in simulations with similar Mg^{2+} and Na^+ concentrations, the model predicted an e-fold change in current for approximately 20 mV and a reversal potential of +6 mV.

Effect of replacing internal Na^+ with Ca^{2+}

Figure 12 shows excised patch currents at +100 mV when the internal solution was 130 mM-NaCl, isotonic $CaCl_2$ (85·7 mM), or a half-and-half mixture of the two solutions. The outward current fell monotonically as Ca^{2+} replaced Na^+, and the ratio of the currents with pure $CaCl_2$ and pure NaCl was about 0·015. Similar results were obtained in three other experiments. This behaviour is similar to that expected from the one-binding-site model (continuous curve in Fig. 12), but different than that of Ca^{2+} channels (see Discussion).

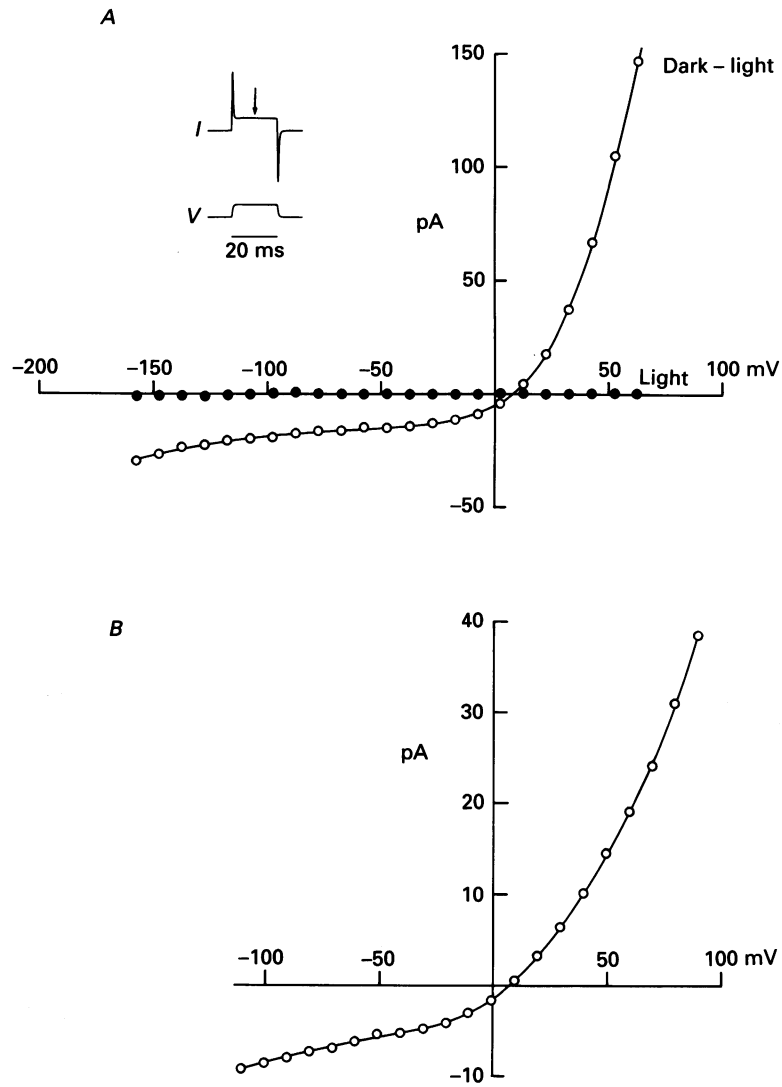

Fig. 11. Comparison of current–voltage relation in the transducing rod with that in an excised patch. Both relations obtained with Ringer solution on the outside and pseudo-intracellular solution on the inside surface of the membrane. Continuous curves drawn by eye. *A*, relation for the light-sensitive current (○, 'dark − light') of an intact, transducing rod, and for its non-light-sensitive leak current obtained in the presence of a saturating light (●, 'light'). Suction electrode currents recorded from the distal half of the outer segment while under voltage clamp by a patch electrode at the inner segment. Low-pass filtered at 1 kHz (−3 dB point, 8-pole Bessel) and sampled at 4 kHz. Leakage conductance 9 pS; reversal potential 7·6 mV; rectification e-fold in 21 mV. Inset: time course of the measured cell membrane current, in response to the indicated jump in membrane voltage, as calculated from the integral of the measured capacity currents; arrow indicates time (10 ms) at which currents were measured to construct the steady-state current–voltage relation. *B*, corresponding relation for an excised patch. Low-pass filtered at 2 kHz (−3 dB point, 8-pole Bessel) and sampled at 10 kHz. Currents in the presence of 1 mM-cyclic GMP minus currents in the absence of cyclic GMP. Measured at 10 ms after switching the voltage. Reversal potential 7·6 mV, seal resistance 10 GΩ, rectification e-fold in 25 mV.

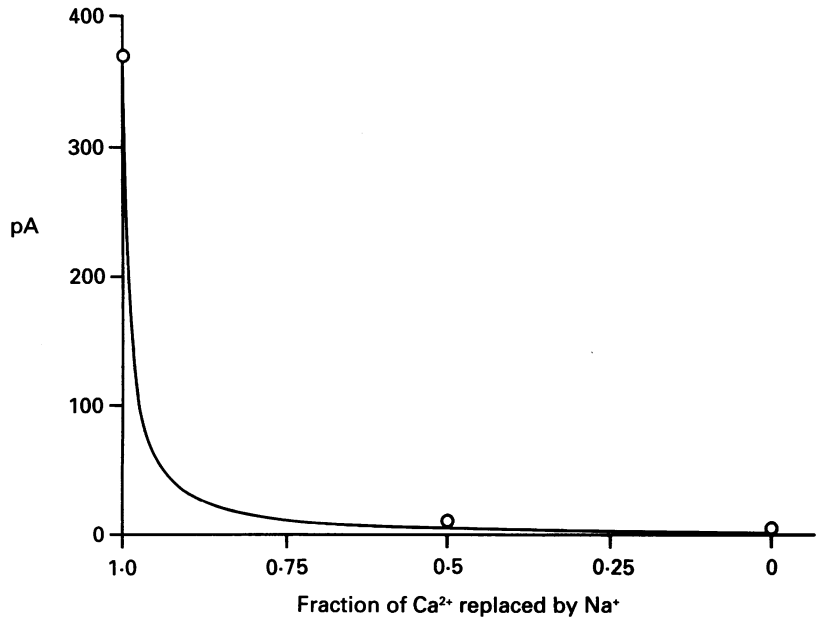

Fig. 12. Outward cyclic GMP-activated currents at +100 mV when internal Na^+ was progressively replaced with internal Ca^{2+}. The three internal solutions were: low divalent 130 mM-NaCl, 65 mM-NaCl with 43 mM-$CaCl_2$, and 85·7 mM-$CaCl_2$. External solution was low divalent 130 mM-NaCl solution. Continuous curve calculated from model with n = 108.

DISCUSSION

One well or multiple wells

The saturation and block in the currents imply that ions bind within the channel, and a model that assumes a single binding site, as used here, is the simplest with a chance to account for these effects. Models based on a single binding site have been used to describe permeation and block in other channels, such as the nicotinic acetylcholine receptor channel (e.g. Lewis & Stevens, 1979; Dani & Eisenman, 1987). Although the one-well model was fairly successful in describing the experimental results, additional binding sites in the channel, especially sites with much higher or lower affinities, are not excluded. Bionic reversal potential measurements at different absolute salt concentrations are more sensitive indicators of the number of ions that can occupy the channel, and experiments of this type have been interpreted to indicate that the cyclic GMP-activated channel can bind more than one ion at a time (Zimmerman & Baylor, 1987; Furman & Tanaka, 1990). Indeed, the model in Fig. 1 predicted current–voltage relations in symmetrical sodium solutions that were somewhat less linear than those actually observed. Extra binding sites tend to linearize the current–voltage relation (Hille, 1984). Menini (1990) has suggested that ions may bind in a vestibule located on the cytoplasmic side of the dominant binding site.

Colamartino, Menini, Spadavecchia & Torre (1990) recently suggested that the cyclic GMP-activated channel contains two binding sites because Ca^{2+} blocked the

channel more strongly than Mg^{2+} at a voltage of -100 mV while Mg^{2+} blocked more strongly at $+100$ mV. Similar effects were observed here (Figs 7 and 8) but can be explained by a one-site model with asymmetric barriers.

In calcium channels repulsive interactions between ions at two binding sites are thought to be crucial for conduction and mediate the large, selective calcium fluxes that occur even in the presence of high concentrations of sodium (Almers & McCleskey, 1984; Hess & Tsien, 1984). None of the results in the present study suggest that this mechanism of conduction operates in the cyclic GMP-activated channel. Although divalent cations carried current through the open channel and strongly inhibited Na^+ fluxes, the divalent currents were very small under all conditions. As Ca^{2+} replaced Na^+ (e.g. Fig. 12) the current through the channel fell monotonically to a low level with no evidence of anomalous mole-fraction behaviour. Ca^{2+} channels, which are thought to contain two ion binding sites, behave differently in both respects (Almers, McCleskey & Palade 1984). These authors measured current through Ca^{2+} channels at constant $[Na^+]$ and found that as the $[Ca^{2+}]$ was raised the current fell to a minimum, as Na^+ current was blocked, then rose again as Ca^{2+} began to carry the current. Although the $[Na^+]$ was held constant, the current would also have passed through a minimum if Ca^{2+} had replaced Na^+. Furthermore, Ca^{2+} was able to carry larger currents than Na^+ in the Ca^{2+} channel.

From the success of the one-well model we conclude that a single binding site may dominate ionic permeation and block in this channel. It should be noted, however, that Rispoli & Detwiler (1990) reported that in detached rod outer segments perfused with ATP and GTP, the dark current showed anomalous mole-fraction behaviour when the $[Ca^{2+}]_o$ was rapidly changed. This behaviour suggested ionic repulsion between calcium ions bound at two sites. Anomalous mole-fraction behaviour was not seen in the absence of nucleoside triphosphates.

Nature of the binding site and barriers

Permeability sequences with monovalent cations suggest that the well in the channel is a 'high field strength' site (Menini, 1990; Furman & Tanaka, 1990), i.e. one with a high negative charge density. Such a site has a higher affinity for divalent cations than for monovalents, causing divalents to pass through the channel relatively slowly. The energy barriers in the model may reflect several factors that impede ion entry, such as steric hindrance and dehydration. An essential feature of our one-site model is that the ratio of the internal and external barrier heights is less than one for Mg^{2+} and more than one for Ca^{2+}. It is this feature that produces the opposite voltage sensitivity for the block of Na^+ current by internal Mg^{2+} and Ca^{2+}.

Relation to channel properties in transducing rods

Under physiological conditions in the transducing rod, the inward current through the light-sensitive channel has been found to be carried by Na^+, Ca^{2+} and Mg^{2+} in proportions of about 1:0·15:0·05 respectively (Nakatani & Yau, 1988); McNaughton (1989) found a ratio of 1:0·1 for Na^+ and Ca^{2+}. Assuming a membrane potential of -35 mV, an external solution containing 110 mM-Na^+, 1·6 mM-Mg^{2+} and 1·0 mM-Ca^{2+}, and neglecting internal concentrations, our model predicts that the relative currents carried by Na^+, Ca^{2+} and Mg^{2+} will be 1:0·044:0·016. The theoretical Ca^{2+} current is

about 3 times larger than the Mg^{2+} current, as observed experimentally, although both theoretical divalent currents are 2–3 times smaller than the experimental divalent currents. The discrepancy may arise from the fact that the model was developed to account for results obtained at saturating cyclic GMP concentration, while in a transducing rod the cyclic GMP concentration is far below saturating (see Yau & Baylor, 1989 for review). The apparent affinity of the binding site for divalent cations is higher at low cyclic GMP concentration (Karpen *et al.* 1988*b*), and indeed in intact rods the relative currents carried by monovalent and divalent cations seem to depend on the internal concentration of cyclic GMP (Cervetto, Menini, Spadavecchia & Torre, 1988).

Another prediction of the model is that at −35 mV, and with the ionic concentrations assumed above, the Na^+ current through the channel will be 340 times smaller under physiological conditions than when divalents are absent. An effective single channel current of a few picoamps has been derived from noise analysis on transducing rods (Bodoia & Detwiler, 1985; Gray & Attwell, 1985; Zimmerman & Baylor, 1985), and this figure fits with the calculated degree of block and a single-channel current in the picoamp region without external divalents (Haynes *et al.* 1986; Zimmerman & Baylor, 1986; Matthews, 1987).

The current–voltage relation of the outer segment exhibits marked outward rectification. Using intracellular microelectrodes, Bader, MacLeish & Schwartz (1979) reported that the outward current increased e-fold for 25 mV of depolarization, and Baylor & Nunn (1986) reported an e-fold increase in 12–14 mV. Using patch-clamp techniques, we have found rectification that is e-fold in 17 mV for transducing rods and e-fold in 24–30 mV in excised patches studied with the same (approximately physiological) solutions. The shallower rectification in excised patches may arise because the voltage dependence of channel gating (Karpen *et al.* 1988) enhances the rectification of a transducing rod, in which the [cyclic GMP] is relatively low, but makes little contribution to the rectification seen in excised patches studied at saturating [cyclic GMP]. It was not feasible to study excised patches with both low [cyclic GMP] and millimolar levels of divalents, since the currents were too small under these conditions. The increase in inward current measured in cells and patches at potentials negative to about −50 or −60 mV may reflect a relief of block by divalent cations at very negative voltage.

Supported by grants EY01543 and EY07774 from the National Eye Institute, United States Public Health Service. We thank Drs Richard Aldrich, Leon Lagnado, and Markus Meister for comments on the manuscript, Ms Sharona Gordon for assistance in some of the experiments, and Mr Robert Schneeveis for excellent technical assistance.

REFERENCES

ALMERS, W. & MCCLESKEY, E. W. (1984). Non-selective conductance in calcium channels of frog muscle: calcium selectivity in a single-file pore. *Journal of Physiology* **353**, 585–608.

ALMERS, W., MCCLESKEY, E. W. & PALADE, P. T. (1984). A non-selective cation conductance in frog muscle membrane blocked by micromolar external calcium ions. *Journal of Physiology* **353**, 565–583.

BADER, C. R., MACLEISH, P. R. & SCHWARTZ, E. A. (1979). A voltage-clamp study of the light response in solitary rods of the tiger salamander, *Journal of Physiology* **296**, 1–26.

BARTFAI, T. (1979). Preparation of metal–chelate complexes and the design of steady-state kinetic experiments involving metal nucleotide complexes. In *Advances in Cyclic Nucleotide Research*, vol. 10, ed. BROOKER, G., GREENGARD, P. & ROBINSON, G. A., pp. 219–242. Raven Press, New York.

BAYLOR, D. A. & NUNN, B. J. (1986). Electrical properties of the light-sensitive conductance of salamander rods. *Journal of Physiology* **371**, 115–145.

BODOIA, R. D. & DETWILER, P. B. (1985). Patch-clamp recordings of the light-sensitive dark noise in retinal rods from the lizard and frog. *Journal of Physiology* **367**, 183–216.

CERVETTO, L., MENINI, A., RISPOLI, G. & TORRE, V. (1988). The modulation of the ionic selectivity of the light-sensitive current in isolated rods of the tiger salamander . *Journal of Physiology* **406**, 181–198.

COLAMARTINO, G., MENINI, A., SPADAVECCHIA, L. & TORRE, V. (1990). Divalent cations currents through cyclic GMP-activated channels from retinal rods. *Biophysical Journal* **57**, 369a.

DANI, J. A. & EISENMAN, G. (1987). Monovalent and divalent cation permeation in acetylcholine receptor channels. *Journal of General Physiology* **89**, 959–983.

FERSHT, A. (1985). *Enzyme Structure and Mechanism*. W. H. Freeman and Co., New York.

FESENKO, E. E., KOLESNIKOV, S. S. & LYUBARSKY, A. L. (1985). Induction by cyclic GMP of cationic conductance in plasma membrane of retinal rod outer segment. *Nature* **313**, 310–313.

FESENKO, E. E., KOLESNIKOV, S. S. & LYUBARSKY, A. L. (1986). Direct action of cGMP on the conductance of retinal rod plasma membrane. *Biochimica et Biophysica Acta* **856**, 661–671.

FURMAN, R. E. & TANAKA, J. C. (1990). Monovalent selectivity of the cyclic guanosine monophosphate-activated ion channel. *Journal of General Physiology* **96**, 57–82.

GRAY, P. & ATTWELL, D. (1985). Kinetics of light-sensitive channels in vertebrate photoreceptors. *Proceedings of the Royal Society* B **233**, 370–388.

HAMILL, O. P., MARTY, A., NEHER, E., SAKMANN, B. & SIGWORTH, F. (1981). Improved patch-clamp techniques for high-resolution current recording from cells and cell-free membrane patches. *Pflügers Archiv* **391**, 85–100.

HAYNES, L. W., KAY, A. R. & YAU, K.-W. (1986). Single cyclic GMP-activated channel activity in excised patches of rod outer segment membrane. *Nature* **321**, 66–70.

HESS, P. & TSIEN, R. W. (1984). Mechanism of ion permeation through calcium channels. *Nature* **309**, 453–456.

HILLE, B. (1975). Ionic selectivity, saturation, and block in sodium channels. A four-barrier model. *Journal of General Physiology* **66**, 535–560.

HILLE, B. (1984). *Ionic Channels of Excitable Membranes*. Sinauer Associates, Sunderland, MA, USA.

HODGKIN, A. L. & HUXLEY, A. F. (1952). Currents carried by sodium and potassium ions through the membrane of the giant axon of *Loligo*. *Journal of Physiology* **166**, 449–472.

KARPEN, J. W., ZIMMERMAN, A. L., STRYER, L. & BAYLOR, D. A. (1988*a*). Gating kinetics of the cyclic-GMP-activated channel of retinal rods: flash photolysis and voltage-jump studies. *Proceedings of the National Academy of Sciences of the USA* **85**, 1287–1291.

KARPEN, J. W., ZIMMERMAN, A. L., STRYER, L. & BAYLOR, D. A. (1988*b*).Molecular mechanics of the cyclic-GMP-activated channel of retinal rods. *Cold Spring Harbor Symposium on Quantitative Biology* **53**, 325–332.

KAUPP, U. B., NIIDOME, T., TANABE, T., TERADA, S., BONIGK, W., STUHMER, W., COOK, N. J., KANGAWA, K., MATSUO, H., HIROSE, T., MIYATA, T. & NUMA, S. (1989). Primary structure and functional expression from complementary DNA of the rod photoreceptor cyclic GMP-gated channel. *Nature* **342**, 762–766.

LAMB, T. D. & PUGH, E. N. JR (1990). Physiology of transduction and adaptation in photoreceptors. *Seminars in the Neurosciences* **2**, 3–13.

LEWIS, C. A. & STEVENS, C. F. (1979). Mechanism of ion permeation through channels in a postsynaptic membrane. In *Membrane Transport Processes*, vol. 3, ed. STEVENS C. F. & TSIEN R. W., pp. 131–151. Raven Press, New York.

MACINNES, D. A. (1961). *Principles of Electrochemistry*, pp. 164 and 167. Dover Publications, Inc., New York.

MCNAUGHTON, P. A. (1989). Role of Ca^{2+} in the light response of vertebrate photoreceptors. *Biophysical Journal* **55**, 581a.

MATTHEWS, G. (1987). Single-channel recordings demonstrate that cyclic GMP opens the light-sensitive ion channel of the rod photoreceptor. *Proceedings of the National Academy of Sciences of the USA* **84**, 299–302.

MENINI, A. (1990). Currents carried by monovalent cations through cyclic GMP-activated channels in excised patches from salamander rods. *Journal of Physiology* **424**, 167–185.

NAKATANI, K. & YAU, K.-W. (1988). Calcium and magnesium fluxes across the plasma membrane of the toad rod outer segment. *Journal of Physiology* **395**, 695–729.

RISPOLI, G. & DETWILER, P. B. (1990). Nucleoside triphosphates modulate the light-regulated channel in detached rod outer segments. *Biophysical Journal* **57**, 368a.

YAU, K.-W. & BAYLOR, D. A. (1989). Cyclic GMP-activated conductance of retinal photoreceptor cells. *Annual Review of Neuroscience* **12**, 289–327.

YAU, K.-W., MCNAUGHTON, P. A. & HODGKIN, A. L. (1981). Effects of ions on the light-sensitive current in retinal rods. *Nature* **292**, 502–505.

ZIMMERMAN, A. L. & BAYLOR, D. A. (1985). Electrical properties of the light-sensitive conductance of salamander retinal rods. *Biophysical Journal* **47**, 357a.

ZIMMERMAN, A. L. & BAYLOR, D. A. (1986). Cyclic GMP-sensitive conductance of retinal rods consists of aqueous pores. *Nature* **321**, 70–72.

ZIMMERMAN, A. L. & BAYLOR, D. A. (1987). Interactions of cations with the cyclic GMP-sensitive channel of retinal rods. *Biophysical Journal* **51**, 17a.

ZIMMERMAN, A. L. & BAYLOR, D. A. (1988). Ionic permeation in the cGMP-activated channel of retinal rods. *Biophysical Journal* **53**, 472a.

ZIMMERMAN, A. L., KARPEN, J. W. & BAYLOR, D. A. (1988). Hindered diffusion in excised membrane patches from retinal rod outer segments. *Biophysical Journal* **54**, 351–355.